Solar cell studies on CuIn$_{1-x}$Ga$_x$Se$_2$ nanoparticles derived from chemical reduction process

Priyanka U. Londhe, Ashwini B. Rohom, Nandu B. Chaure*

Department of Physics, Savitribai Phule Pune University (formerly University of Pune), Pune 411007, India

ABSTRACT

Precisely controlled copper indium gallium diselenide (CuIn$_{1-x}$Ga$_x$Se$_2$; x = 0 to 1) nanoparticles (NPs) are synthesized by using a simple low-cost, environment friendly chemical ion reduction method. A versatile polyethylene glycol (PEG) is used as solvent as well as stabilizer, which allowed the synthesis of NPs at higher working temperature (~300 °C). CuIn$_x$Ga$_{1-x}$Se$_2$ NPs with precisely controlled properties and high degree of crystallinity are reported. The samples revealed tetragonal crystal structure with systematic variation in 'd' values for (1 1 2) reflection demonstrate the synthesis of CIS, CIGS and CGS. The variation in the interplanar distances 'd' for (1 1 2) is further confirmed with HRTEM analysis. The sharp spotted rings observed from SAED pattern demonstrate the polycrystalline grwoth of CuIn1$_{-x}$Ga$_x$Se$_2$ NPs. Non-uniform CuIn$_x$Ga$_{1-x}$Se$_2$ NPs of size ranging from 20 to 100 nm are observed from TEM analyses. However, upon annealing the final devices at 450 °C for 20 min. the NP layers become the polycrystalline alloy of materials with uniform cluster size between 100 and 200 nm. The optical absorption results revealed the addition of Ga in the crystal structure with systematic blue shift in the absorption wavelength. The superstrate solar cell developed from CIS, CIGS and CGS NPs measured efficiency 7.80, 9.33 and 9.04%, respectively upon illumination with 100 mW/cm^2. The yield of NPs was over 90%, therefore, the synthesis procedure may be suitable for commercialization purpose and for preparation of flexible solar cells.

1. Introduction

In spite of the highest power conversion efficiency (PCE), 23.3 and ~18.6% for lab scale solar cell devices and module, respectively (Green et al., 2020) with excellent execution of copper indium gallium di-selenide (CIGS) thin film solar cells (TFSC) to date, conventional vacuum-based fabrication methods are restricted to an extensive commercialization due to the high production cost. Additionally, the massive capital investments, high purity precursor recourses, low-deposition rate, wastage of materials during deposition, etc. are some of the critical issues of vacuum based growth techniques. With this perspective CIGS layers have been obtained by using environmental friendly chemically prepared nano-ink with spray coating (Ahn et al., 2009), spin coating (Liu et al., 2012), and doctor blade-deposition (Kaelin et al., 2004) methods are followed post-deposition heat treatment in controlled ambient or selenium atmosphere. These routes are considered to be a promising due to being simple and low-cost methods with feasibility for scaling up. The ink of CuIn1$_{-x}$Ga$_x$Se$_2$ nanoparticles (NPs) is one of the best options to produce TFSCs with high purity and controllable stoichiometry. The lower melting temperature of NPs as a counter part of bulk

is also beneficial towards the development of high PCE devices (Wang and Xia, 2004). Nevertheless, the carbon resided from organic binder remains in CIGS thin films despite of heat treating for high temperatures. This residue not only causes high series resistance in solar cell devices but also leads to the poor adhesion of thin films to the substrate, which degrade the performance and stability (Kaelin et al., 2005). Many researchers have devoted their efforts to produce the TFSCs with the ink of CIGS NPs. Several attempts have been made in the literature to obtain high quality CIGS thin films by various techniques. Commonly, two ways are accepted for the development of nanoparticle-based solar cell; first is the preparation of precursor layer using the CIGS powders and second is the mechanical alloying. The sintering procedure on the above sample leads to obtain a dense and well-adherent absorber layer. NPs of CIS and its combinations had been successfully used in quantum dot based solar cells (Peng et al., 2017; McDaniel et al., 2013; Chang et al., 2013), dye sensitized solar cells (Wu et al., 2017), photo-detectors (Sargent et al., 2010), water splitting (Septina et al., 2015) and in biological imaging as fluorescence material (Cassette et al., 2010).

Several chemical routs have been employed for the synthesis of

---

* Corresponding author.
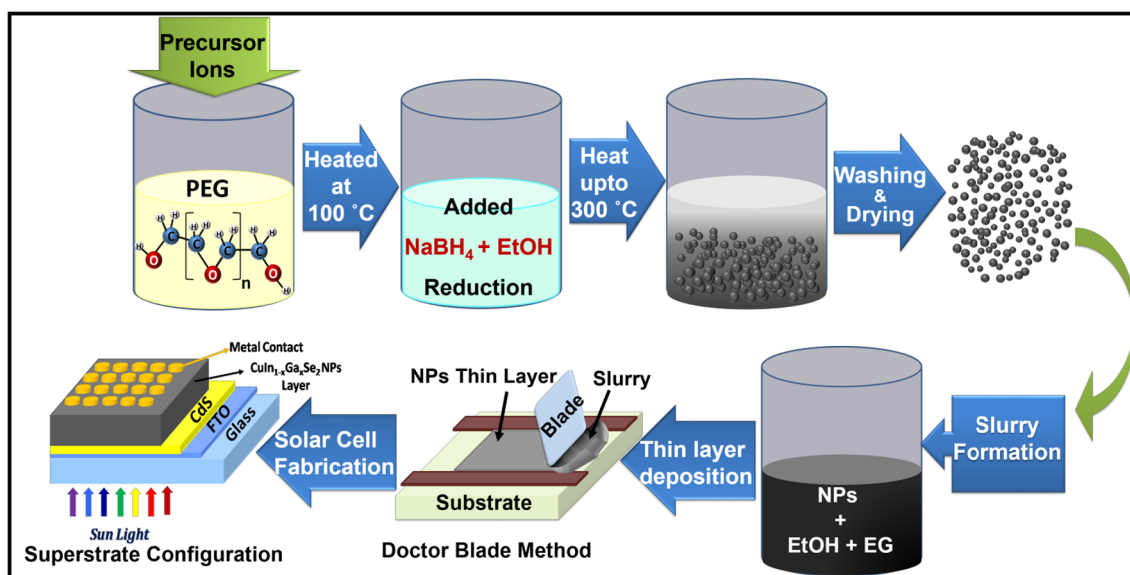 *E-mail address:* n.chaure@physics.unipune.ac.in (N.B. Chaure).

Fig. 1. Schematic of steps involved in the synthesis and development CuIn$_{1-x}$Ga$_x$Se$_2$ NPs superstrate solar cell.

CuIn$_x$Ga$_{1-x}$Se$_2$ NPs such as, solvothermal, hot injection, microwave synthesis, colloidal solution-phase growth, hydrothermal, chemical reaction and ball milling. CIGS NPs were initially prepared by Schulz et al. (1998) using colloidal formation method using iodide precursors in methanol solvent and reported 4.6% PCE onto Mo coated glass substrates. CuGaS$_2$ NPs were synthesized by Gurin et al. by using the nitrate of Cu and Ga as precursors with hydrogen sulfide/selenide (Gurin, 1998). CIGS NPs synthesized by Barbé et al. (2016) with various ratios of Cu/(Ga + In) have reported 6.5% PCE for the printed cells onto Mo substrate. Some reports are also available on the synthesis of submicron size CIGS particles using mechano-chemical synthesis with disciplined ball milling of metallic precursors (Liu and Chuang, 2012; Rohini et al., 2015). Sono-chemical route with hydrazine based solvents was employed by Cha et al. (2015) for the synthesis of CIGS NPs. The synthesis of CuInS$_2$ nanorods from aqueous solution at low temperature is reported by Xiao et. al. (Xiao et al., 2001). Gou et al. described the synthesis of CIS nanorings and CIGS nanocrysatls by hot injection method with two different solvents, oleylamine (OLA) and o-di-chlorobenzene (DCB) and reported the cells with ~12% PCE (Guo et al., 2008; Guo et al., 2013). Although the results are good, however the complicated steps involved in synthesis process of NPs are not suitable for mass production. Panthani et al. have reported the optimized parameters for the synthesis of different shape and size of CIS, CGS and CIGS NPs (Panthani et al., 2008). The conditions for synthesis of different shaped CIS, CIGS and CGS NPs, like spherical, triangle, plates, etc. have been reported by Tang et al. (2008). Also, several other reports are available in the literature for synthesis of chalcopyrite NPs using similar non-coordinating solvents. However, the residual C-containing compound and high cost of these solvents are the some of the critical issues in solar cells development. The preparation of CIGS NPs with modified polyol route is reported by Wu et al (Wu et al., 2012). Mitzi et. al and Mcleod et al. have established the hydrazine based procedure to develop the CIGS NP ink and reported15.2 and 15% PCE solar cells (Mitzi et al., 2009; McLeod et al., 2015). Nansolar has developed 15.3% efficient CIGS cells by mixing the NPs with selenide.

We focus to develop a simple, cost-effective, rapid metal ion reduction technique for synthesise of stoichiometric CuIn$_{1-x}$Ga$_x$Se$_2$ NPs with high yield. Herein, attempts have been made to prepare these NPs by less toxic and reasonably fast chemical reaction method and a simple p-n heterojunction superstrate (FTO/CdS/CIGS/Au) solar cell structure is fabricated. The glycols and their derivative can serve as a solvent, soft-reductant and stabilizer. The oxidation of glycol gives glycolate

which sometimes may stabilize the NPs without additional stabilizer (Lee et al., 2012; Tsuji et al., 2004). Since the glycols are soft-reductant (Santaniello et al., 1987) the reduction of metallic ions from polyol substances requires more kinetic energy, like microwave irradiation (Lebègue et al., 2011). PEG is used as solvent as well as stabilizer to prevent the agglomeration of nanostructures and NaBH$_4$ plays a role of strong reducing agent. The performance of superstrate devices fabricated using CIS, CIGS and CGS NPs are reported.

2. Materials and methods

2.1. Materials

Copper chloride (CuCl$_2$), indium chloride (InCl$_3$), gallium chloride (GaCl$_3$) and selenium tetrachloride (SeCl$_4$) were used as resources to Cu, In, Ga and Se, respectively. PEG-400 was used as solvent as well as stabilizer. Sodium borohydrate (NaBH$_4$) was used as reducing agent. All chemical were procured from Sigma-Aldrich with purity at least 99% and used as received without purification.

A simple, cost-effective and environment friendly chemical reduction method was employed for synthesize of CuIn$_{1-x}$Ga$_x$Se$_2$ NPs. A solution was prepared by dissolving the precursors of Cu, In Ga and Se with molar ratios 1 : 1-x : x : 2 respectively, where x ranging from 0 to 1 in 50 ml of PEG. A clear solution was obtained at temperature 100 °C with continuous moderate stirring within two hours. Subsequently, NaBH$_4$ was added in the above solution and raised the temperature slowly (2 °C/min) upto 300 °C. Upon completing the chemical reaction in few hours a dark brownish colored solution was obtained. A homogenous solution became precipitate upon adding the desired amount of ethanol. The final product was centrifuged several times at 10,000 rpm for 10 min. Upon cleaning and drying at ambient condition a greyish-black powder was obtained. These samples were dispersed in water and chloroform for further characterizations. It is noteworthy that the NPs prepared by above procedure yields over 90%.

The homogeneous slurry of CuIn$_{1-x}$Ga$_x$Se$_x$ NPs was prepared by dispersing the powder sample into ethylene glycol and ethanol with optimized ratio. The slurry of CuIn$_{1-x}$Ga$_x$Se$_x$ NPs was uniformly coated onto CdS window layer having dimensions 2 cm × 3 cm by doctor blade method. The thicknesses of absorber layer were measured to be ~2.5 μm (± 100 nm) by Filmetrics F-10 thin film analyzer. The thickness of CIS, CIGS and CGS was kept similar for the characterization and fabrication of solar cell devices. CdS layers of thickness ~80 nm
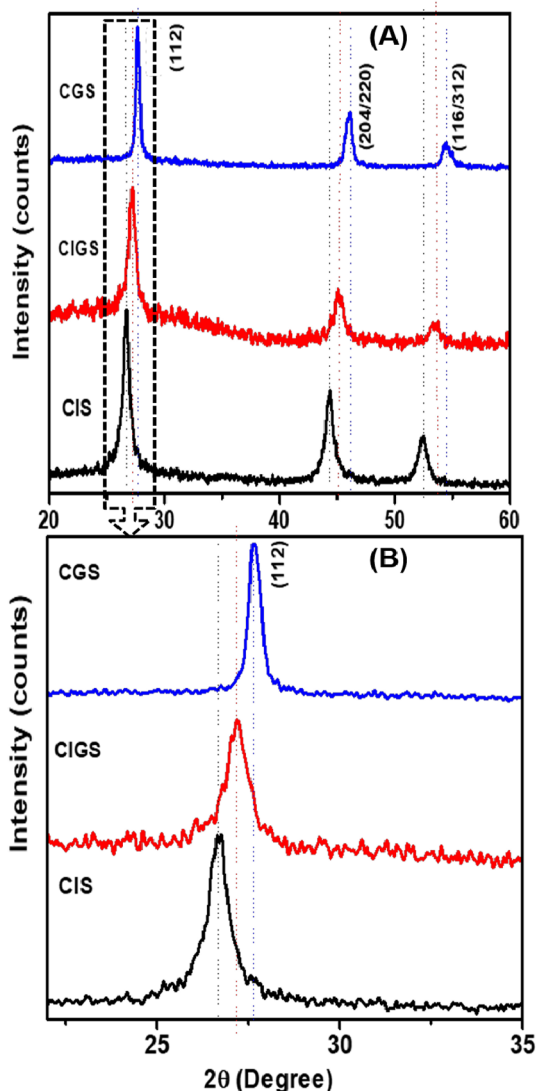
Fig. 2. (A) XRD pattern of as-prepared $CuIn_xGa_{1-x}Se_2$ NPs obtained for different precursor concentrations, (B) A magnified image of (1 1 2) Bragg reflection of CIS, CIGS and CGS NPs.

(± 10 nm) were deposited by chemical bath deposition technique onto transparent conducting fluorine doped tin oxide (FTO) coated glass substrates (Chaure et al., 2003). Final devices were annealed in Argon ambient at 450 °C for 20 min. A home-made thermal evaporation with vacuum ~10^{-6} mbar was employed for evaporation of Au-metal electrodes of 3 mm diameter on $FTO/CdS/CuIn_{1-x}Ga_xSe_2$ structure. Prior to metal contact, the samples were chemically etched with Br_2/Methanol and NaCN solutions for 30 sec each. The various steps involved

for synthesis of $CuIn_{1-x}Ga_xSe_2$ NPs and preparation of superstrate solar cells structure is represented in Fig. 1.

2.2. Characterization techniques

The as-prepared $CuIn_{1-x}Ga_xSe_2$ NPs were characterized with a range of characterization techniques to examine the various properties of material. The structural properties were studied using Diffractometer, D8 Advanced, Bruker AXE Germany with Cu Kα radiation (wavelength of 1.5405 Å). UV–Vis-NIR spectrophotometer, Model, JASCO V-770 was employed to examine the optical properties. The surface topographical variation was closely examined by using the scanning electron microscope (SEM), Model, JEOL JSM-6360A with an operating voltage 20 kV. The elemental atomic percentage composition of NPs was determined with the help of energy dispersive spectroscopy (EDS) technique equipped with above SEM instrument. The transmission electron microscopy (TEM), TECNAI G^2 with an operating voltage 200 kV was employed to the shape and size of NPs and related crystallographic information. X-ray Photoelectron Spectra (XPS) were recorded by PHI 5000 Versa Probe II (Al Kα (1486.6 eV) X-ray source) spectrometer to study chemical states. The illuminated current density-voltage characteristics measurements were carried out at room temperatures with input power density, 100 mW/cm^2 (1.5 AM). Photon counting spectrometer, ISS Inc., along with Kiethley 2400 source meter was used to measure the external quantum efficiency (EQE).

3. Results and discussion

3.1. Characterization of CIS/CIGS/CGS NPs

3.1.1. Structural analyses

The XRD patterns shown in Fig. 2 for as-prepared $CuIn_{1-x}Ga_xSe_2$ (x = 0, 0.5 and 1) NPs exhibited three prominent reflections, (1 1 2), (204/220) and (3 1 2)/(1 1 6) corresponds to tetragonal crystal structure of $CuIn_{1-x}Ga_xSe_2$. The (1 1 2) reflections observed about 2θ = 26.63°, 27.21°and 27.70° with x = 0, 0.5 and 1.0, respectively are associated CIS (JCPDS NO. 81-1936), CIGS (JCPDS NO. 40-1488) and CGS (JCPDS NO. 35-1100). A clear shift in the position of (1 1 2) can be clearly seen in the magnified image (Fig. 2B) upon increase in Ga concentration in the precursor solution. The non existence of metallic and/or binary/ternary alloy phases in XRD data illustrates the precision in synthesis procedure. The broadening in XRD peaks clearly confirms the synthesis of NPs. The differences in d-values could be associated to the strain developed onto the crystal lattice. The substitution of Ga at the site of In, may develop the compressive strain on the crystal lattice due to the smaller atomic size (130 pm) than In (155 pm). The values of lattice parameters 'a,' 'c' and 'c/a' calculated from the XRD results tabulated in table 1 are in agreement with the standard lattice values of tetragonal crystal structure CIS, CIGS and CGS. Further, the values of 'a' and 'c' were found to be reduced with increasing the Ga contents. A linear relation observed between the lattice parameters and the amount of x in the $CuIn_{1-x}Ga_xSe_2$ matrix is shown in Fig. 3. This tendency is

Table 1

A summary of the interplanar d and the lattice parameters (a and c) determined for as-prepared $CuIn_{1-x}Ga_xSe_2$ NPs from XRD results. using different techniques in the literature.

Values of x	Binding Energies (eV)[a]							
	Cu $2p_{1/2}$	Cu $2p_{3/2}$	In $3d_{3/2}$	In $3d_{5/2}$	Ga $2p_{1/2}$	Ga $2p_{3/2}$	Se $3d_{3/2}$	Se3 $d_{5/2}$
1	951.5	931.7	451.8	444.3	–	–	55.1	54.1
0.5	951.4	931.8	451.9	444.4	1144.7	1118.9	55.3	54.4
0	951.9	931.2	–	–	1144.3	1118.4	55.7	54.6

[a] Please interchange Table 1 and 2. Table 1 is for XRD data while table 2 for XPS analysis. However their table captions are correct.

Table 2
Summary of the binding energy peaks of Cu2p, Ga2p, In3d, and Se3d observed for CIS, CIGS and CGS NPs from XPS analysis.

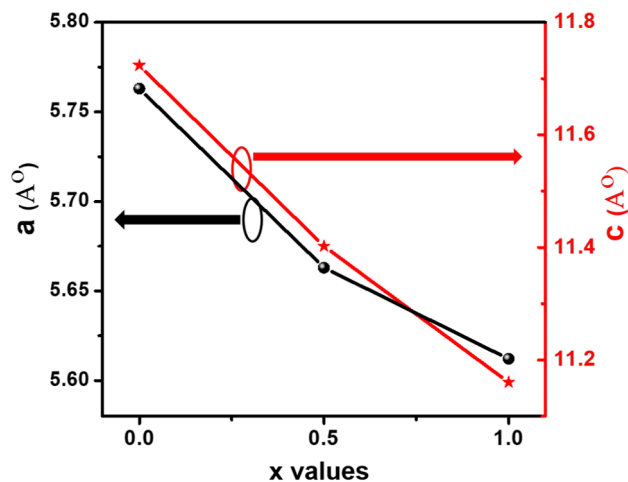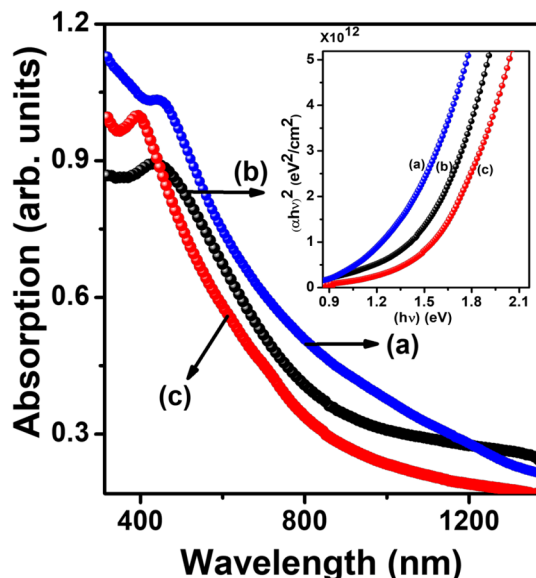| Value of x	Peak (1 1 2) 2θ°	d_{112} (Å)		a (Å)		c (Å)		μ= c/a	
		Standard	Calculated	Standard	Calculated	Standard	Calculated	Standard	Calculated
1	26.65	3.34	3.34	5.78	5.77	11.64	11.68	2.01	2.02
0.5	27.21	3.27	3.27	5.69	5.67	11.32	11.36	1.98	2.00
0	27.70	3.21	3.21	5.61	5.59	11.03	11.20	1.96	2.00

Fig. 3. The dependence of the lattice parameters, '*a*' and '*c*' on the nominal Ga content.

Fig. 4. Optical absorption spectra of CIS, CIGS and CGS NPs. Inset shows the Tauc plots, $(\alpha h\nu)^2$ versus (hν).

coherent with Vegard's law, which supports an evenly In–Ga alloying (Denton and Ashroft, 1991). The lattice distortion obtained for CuIn$_{1-x}$Ga$_x$Se$_2$ NPs ($c/a \approx 2$) was found to be very similar to that of the perfect tetragonal structure (Thomas et al., 2016).

3.1.2. Optical studies

Considering the application of nanomaterials especially semiconductors and plasmonic NPs in optoelectronic devices, energy band gap and optical absorption are the important properties. Spectral response of semiconductor nanomaterials can be achieved by changing the energy band gap upon controlling the size and shape. Optical absorption spectra's of CIS, CIGS and CGS NPs suspended in ethanol solvent studied by UV–Vis-NIR spectrophotometer are shown in Fig. 4. All samples revealed a fine absorption in the visible region, represent a possible application in solar cells. Optical energy band gaps of the CuIn$_{1-x}$Ga$_x$Se$_2$ NPs were estimated by the Tauc equation,

$$\alpha h\upsilon = A(h\upsilon - E_g)^n \tag{1}$$

where α is the absorption coefficient, A is the Richardson's constant, E_g is the energy band gap, h is the Planck's constant, υ is the frequency and n is the variable which depends on the type of transition. Since CIGS is direct band gap semiconductors, therefore, the value of n was taken to be ½. Upon increasing the Ga atoms into the lattice of CuIn$_{1-x}$Ga$_x$Se$_2$ results the blue shift in the optical absorption spectrum. The values of bandgap 1.24, 1.51 and 1.70 eV for CIS, CIGS and CGS, respectively were estimated from the intersect of the extrapolation of linear segment of $(\alpha h\nu)^2$ to the energy axis. The blue shift observed in the absorption edge with increase in Ga concentration can be explained by Moss-Burstein effect which occurs due to the increased carrier concentration either in conduction or valence band leads the shifting of fermi energy level. Upon increasing the Ga concentration the CuIn$_{1-x}$Ga$_x$Se$_2$ becomes the degenerate p-type semiconductor and the fermi level may lies in the valance band. The position of Fermi level depends on Ga concentration. The Ga atoms in CuIn$_{1-x}$Ga$_x$Se$_2$ leads to increase the free charge carrier concentration (i, e, hole) and the highest electronic states of valence band become empty, which shift the absorption edge towards higher photon energy. These values are slightly higher than respective bulk counterpart, which confirms the formation of nanoparticles (Londhe et al., 2015; Ishizuka et al., 2004; Noufi et al., 1986).

3.1.3. TEM analysis

The morphological, structural and compositional studies were performed by using TEM. The bright field images of CIS, CIGS and CGS NPs are shown in Fig. 5(a), (b) and (c), respectively. The partially agglomerated non uniform particles with size ranging from 20 to 100 nm were observed. The non-uniform particles with different sizes could be immaterial for solar cell development because upon annealing the final devices at 450 °C for 20 min. the NP layer may form the polycrystalline alloy of materials. Indeed, after annealing we have noticed the uniform growth of clusters in SEM images due to the lower melting of NPs. The high-resolution transmission electron micrographs (HRTEM) are shown Fig. 5(d), (e) and (f), respectively. The magnified HRTEM images given in the inset of corresponding figure clearly exhibits the crystal planes. The interplanar distance 'd' measured to be approximately 3.45, 3.37 and 3.28 Å for CIS, CIGS and CGS NPs respectively, are similar to the 'd' values of (1 1 2) reflection for respective material. The results obtained in HRTEM are consistent with XRD results.

The selected area electron diffraction (SAED) patterns for CIS, CIGS and CGS NPs are depicted in Fig. 6(a)–(c), respectively. The observed circular spotted rings correspond to (1 1 2), (204/220) and (3 1 2)/ (1 1 6) Bragg reflections of chalcopyrite tetragonal structure of CuIn$_{1-x}$Ga$_x$Se$_2$ (x = 0, 0.5 and 1). The spotted behaviour of ring represents the polycrystalline behaviour of material (Egerton, 2005). The
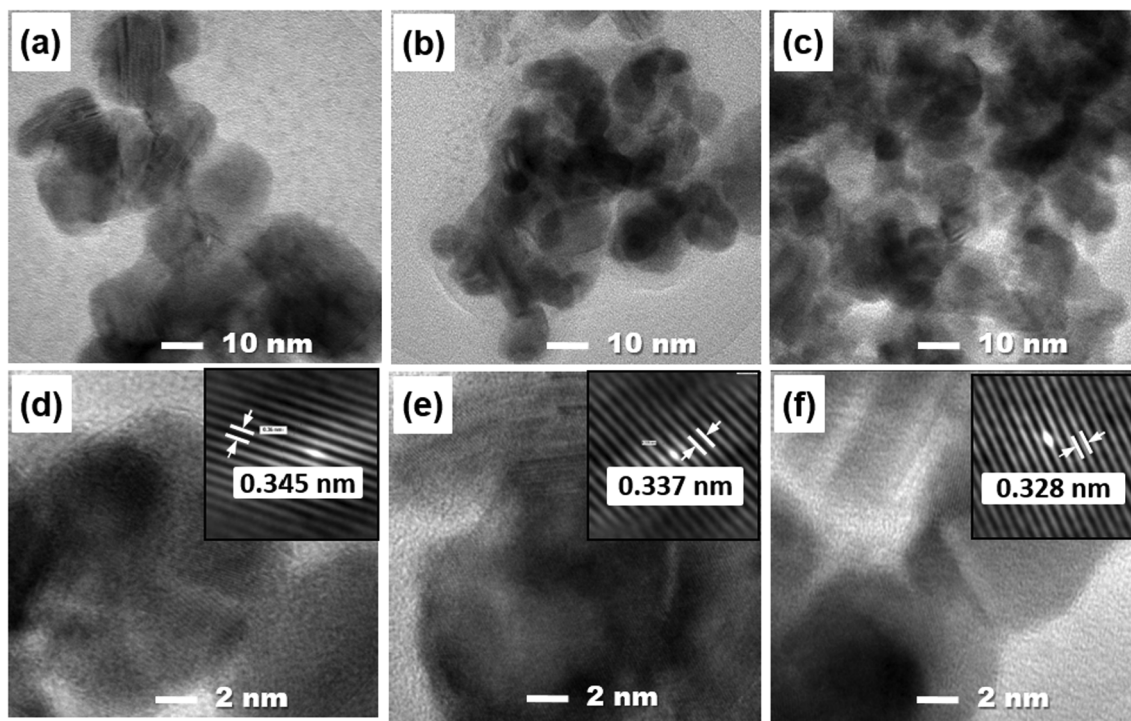
Fig. 5. (a–c) Bright field TEM images and (d–f) HRTEM image of CIS, CIGS and CGS NPs, respectively. Insets are corresponding magnified HRTEM images.
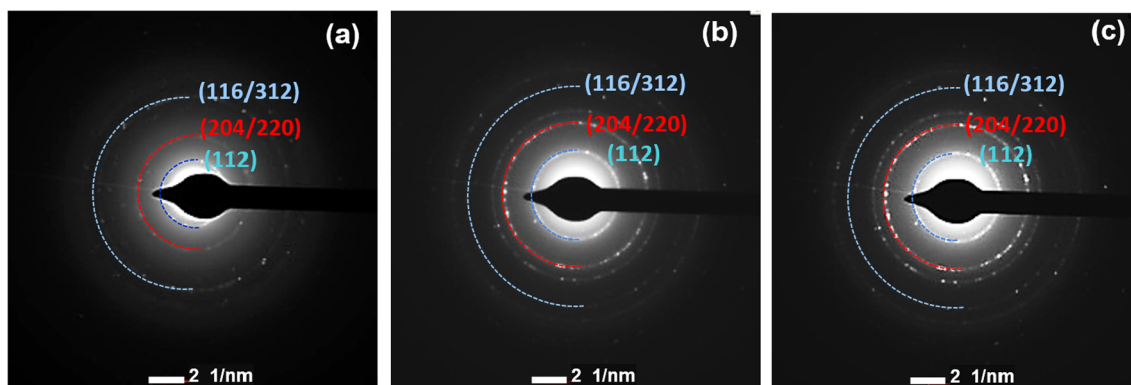

Fig. 6. SAED patterns of as-deposited CIS (a); CIGS (b) and CGS (c) NPs.
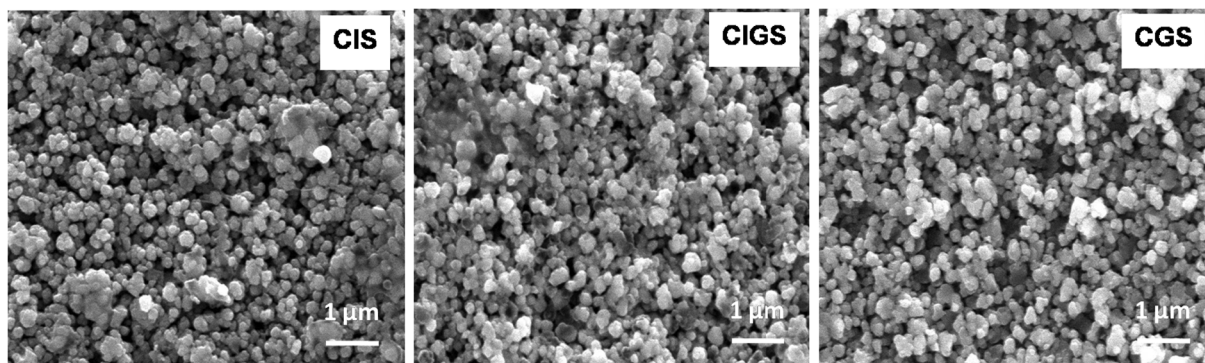

Fig. 7. The topographical SEM images of annealed CIS, CIGS and CGS NP layers prepared by doctor blade method.

Table 3

Atomic percentage composition of as-prepared and annealed $CuIn_{1-x}Ga_xSe_2$ NPs determined by EDS analysis.

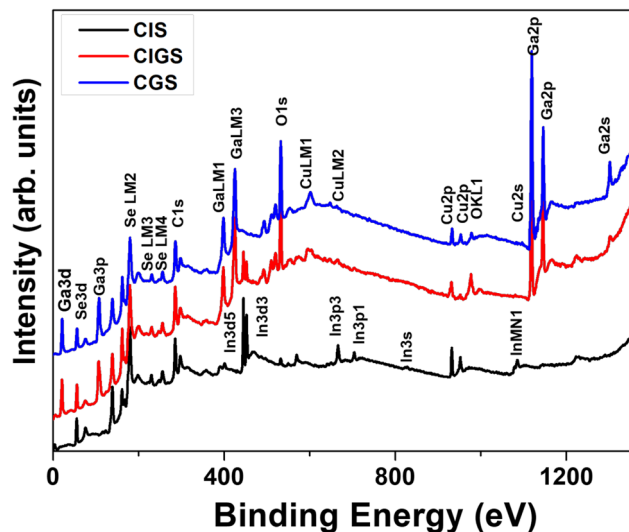| Sample	Atomic Percentage Composition							
	Cu		In		Ga		Se	
	As-prepared	Annealed	As-prepared	Annealed	As-prepared	Annealed	As-prepared	Annealed
CIS	21.54	23.04	23.54	24.12	0	0	54.49	52.84
CIGS	26.85	27.12	10.24	11.13	8.53	8.73	54.39	53.02
CGS	19.82	20.98	0	0	21.44	22.23	58.74	56.79

Fig. 8. XPS survey spectrum for CIS, CIGS and CGS NPs.

topographical SEM mages of the annealed CIS, CIGS and CGS NP devices prepared by doctor blade method are shown in Fig. 7. Upon annealing the NPs gets settled rapidly due to the lower melting point, leading to the formation of clusters of size ~100–200 nm. Compact, densely packed surface morphology without pin holes can be clearly seen in figure. The contrast observed on the surfaces could be due to the uneven texture of the particles; however the textured surface is helpful in superstrate solar cell (Chaure et al., 2004). Nearly similar surface morphology was imaged for CIS, CIGS and CGS samples. The elemental atomic percentage composition of the as-prepared and annealed $CuIn_{1-x}Ga_xSe_2$ NPs determined with the help of EDS technique is given in Table 3. The reported concentrations are the average of three reading taken at different surface areas. Slightly Se-rich NPs were synthesized, however upon annealing the Se contents were found to be reduced probably due to the evaporation of elemental selenium. The annealed NPs of CIS, CIGS and CGS were exhibited nearly stoichiometric composition.

3.1.4. XPS analysis

The chemical states of element in $CuIn_xGa_{1-x}Se_2$ NPs were examined by XPS analyses with monochromatized Al Kα radiation as an excitation source. The XPS survey scan for $CuIn_{1-x}Ga_xSe_2$ NPs shown in Fig. 8 illustrates the presence of Cu, In, Ga and Se without impurities. The core level spectra for Cu, In, Ga and Se of CIS, CIGS and CGS NPs are represented in Fig. 9(a), (b) and (c), respectively. Core level spectra for Cu2p divided into two $2p_{3/2}$ and $2p_{1/2}$ peaks which reveal the +1 valence state of Cu in all $CuIn_{1-x}Ga_xSe_2$ NPs. The splitting of core level spectra of In3d into $3d_{5/2}$ and $3d_{3/2}$ peaks confirmed the +3 valence state of In in CIS and CIGS NPs. Similarly, the splitting of core level spectra of Ga2p into two peaks $2p_{3/2}$ and $2p_{1/2}$ demonstrate the valence

state of Ga in CIGS and CGS is +3. The Se3d peak was de-convoluted in two peaks corresponding to $3d_{5/2}$ and $3d_{3/2}$ levels. The above result confirms the electronic states of Cu, In, Ga and Se in $CuIn_{1-x}Ga_xSe_2$ NPs were Cu^+, In^{3+}, Ga^{3+} and Se^{2-}. The values of binding energy of Cu2p, Ga2p, In3d, and Se3d in CIS, CIGS and CGS are tabulated in table 2.

3.1.5. Optoelectronic properties

The illuminated current density-voltage (J-V) characteristics and quantum efficiency measurement were performed on CdS/$CuIn_{1-x}Ga_xSe_2$ heterojunction devices. The devices were illuminated artificially using solar simulator having input power intensity 100 mW/cm^2. The slurry of $CuIn_{1-x}Ga_xSe_2$ NPs prepared with ethylene glycol and ethanol were applied onto FTO/CdS substrates using doctor blade method. These devices were annealed in Ar ambient at 450 °C for 20 min to remove the traces solvents. Subsequently, the samples were chemically treated in Br/Methanol followed by NaCN solution each for 30 sec to eliminate the oxides and/or binary phases formed during annealing. Prior to apply the slurry of $CuIn_{1-x}Ga_xSe_2$ onto FTO/CdS, the substrates were annealed at 450 °C for 15 min. at ambient condition. Fig. 10 depicts the illuminated J-V characteristics of the CdS/CIS a), CdS/CIGS b) and CdS/CGS c) solar cell devices. The basic solar cell parameters, short circuit current density (J_{sc}), open circuit voltage (V_{oc}), fill factor (FF) and PCE (η) are given in table 4. The cells fabricated using CIGS NPs were measured highest PCE ~ 9.33%. A low value of FF was found to be affected on the performance of devices. The FF can be improved by optimising the proportion of binder, complete removal binder, which will reduce the series resistance of the device. Upon increasing Ga concentration in the $CuIn_{1-x}Ga_xSe_2$ matrix, the values of V_{oc} were found to be increased due to the increased bandgap of absorber layer. Conversely, the decreased value of J_{SC} upon increasing Ga content could be due to the reduced depletion width causing reduction in carrier collection probability (Kodigala, 2010). The measured device parameters are compared with the previously reported CIGS NP solar cells in table 5. This comparative study clearly demonstrates that the efficiency of the CIS, CIGS and CGS NPs solar cells reported in present study is higher than the reported values of CIGS NPs-based devices in the literature (Mousavi et al., 2016; Tuan et al., 2017; CheshmeKhavar et al., 2017; Badgujar et al., 2018).

The results obtained with illuminated condition for $CuIn_{1-x}Ga_xSe_2$ based solar cells are further verified by using external quantum efficiency (EQE) measurements. Fig. 11 shows the EQE curves measured for solar cell devices fabricated with CIS, CIGS and CGS NPs. All devices measured around 80% EQE for the region 550–750 nm. The low EQE recorded for region 400–530 nm is proposed due to the absorption loss in CdS window layer. The increase in the short circuit current density for CIS and CIGS devices could be associated to the enhancement of EQE in the long wavelength region. The blue shift observed in the onset of absorption wavelength confirms the presence of Ga in the sample, which is associated to the band edge transition of material. A Tauc plot, $(E \times EQE)^2$ versus band energy (hν) given in the inset of Fig. 11 yields the bandgaps 1.20, 1.49 and 1.56 eV for CIS, CIGS and CGS,
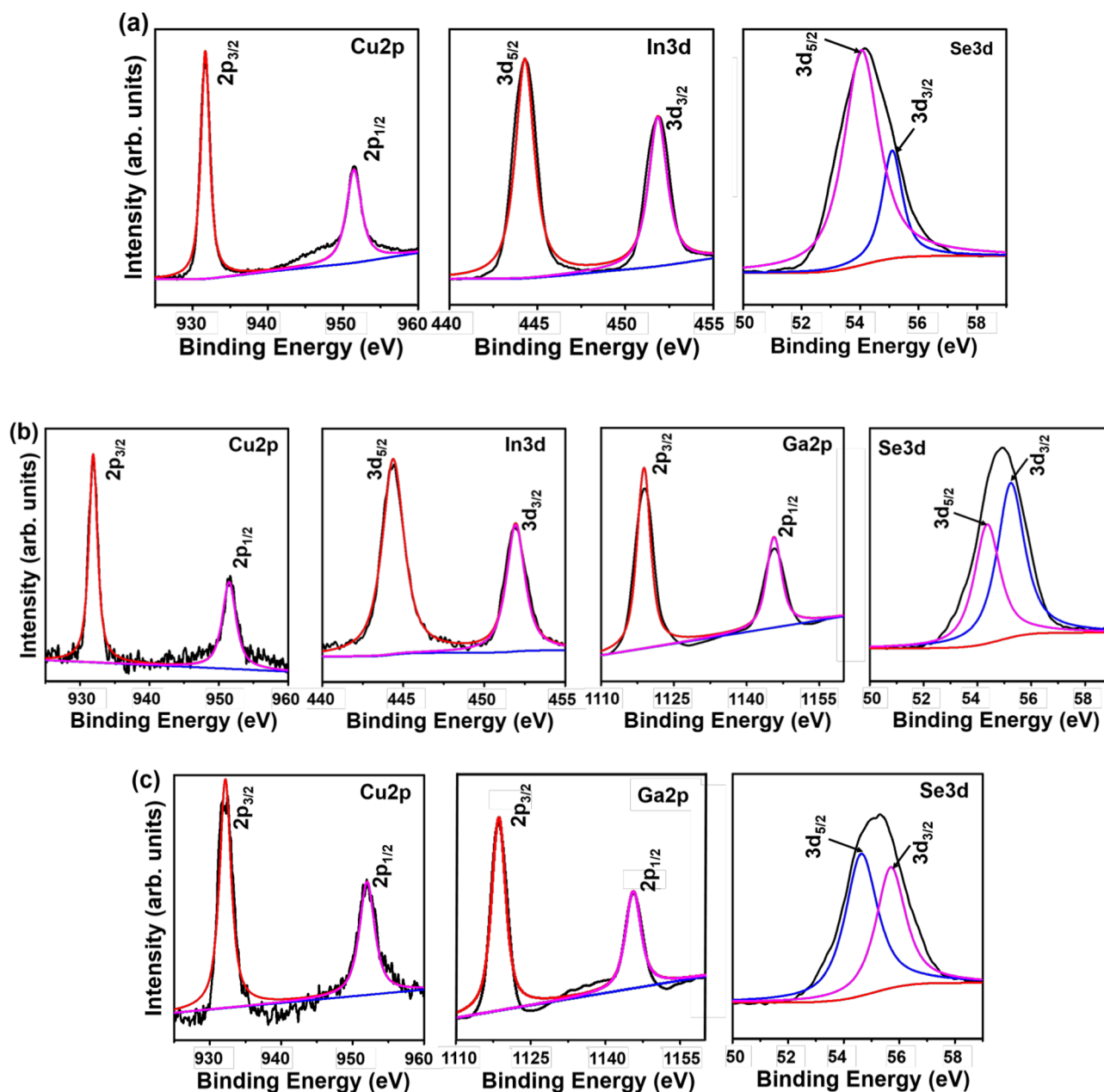
Fig. 9. Core level spectra's for Cu, In Ga and Se in (a) CIS, (b) CIGS and (c) CGS NPs.

respectively, which are close to the values of polycrystalline alloy materials. The deviation noticed in the bandgaps as compared with the values estimated from absorption spectra could be due to the improvement in particles size by agglomeration, re-crystallization and a slight change in the elemental composition of layer upon annealing. A slight difference in the slope observed for CIS sample could be attributed to the more collection of photons.

The less PCE measured for CIS and CGS cells could be due to, (i) higher defect density (bulk) in space charge region, (ii) grain boundaries, (iii) surface defects, (iv) insufficient absorption of photon, (v) recombination of charge carriers through the defects at the junctioninterface. The CGS cells showed slightly less EQE than the CIS and CIGS which could be due to the less J_{SC}. It is also reported that, with increasing the Ga content, the density of defect levels increases (Chen et al., 1993; Basol et al., 1996); which could limits the J_{SC}. The band

gap of CGS (~1.70 eV) could be another factor for limiting the efficiency, which contributes negligible absorption of photons above 800 nm. The higher Cu/In ratio obtained for CIS as compared to CIGS and CGS could be responsible to measure the low efficiency by generating the higher surface as well as bulk defects (Unold et al., 2006). It is also reported that the higher concentration of In in CIGS can produce the planner defects (Alberts et al., 1997). The band tailing observed in EQE spectra at infrared region (< 900 nm) for the CIS, clearly confirms the presence of defect states. This band tailing causes due to the optical transitions in between valence band to defects or defects to conduction band or vice versa, rather than direct band to band transition. The lower band gap of CIS as compared to the optimum band gap for high efficiency solar cell (~1.40 eV) by Schockley-Queisser limit, could be one of the reasons to measure less efficiency (Schockley et al., 1961).
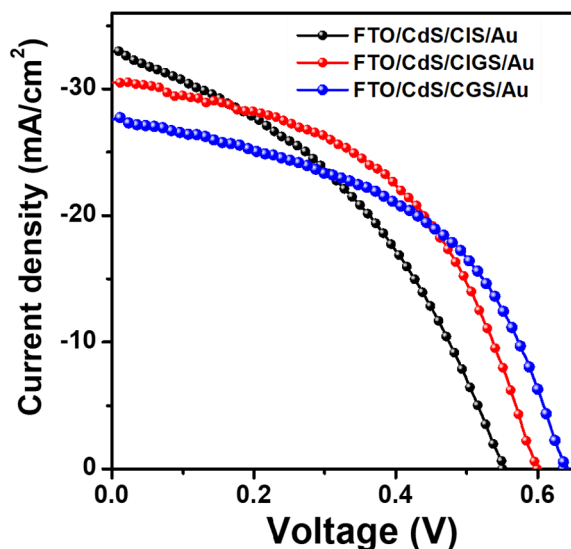
Fig. 10. J-V characteristics of (a) CIS, (b) CIGS and (c) CGS NPs based super-strate solar cell devices.
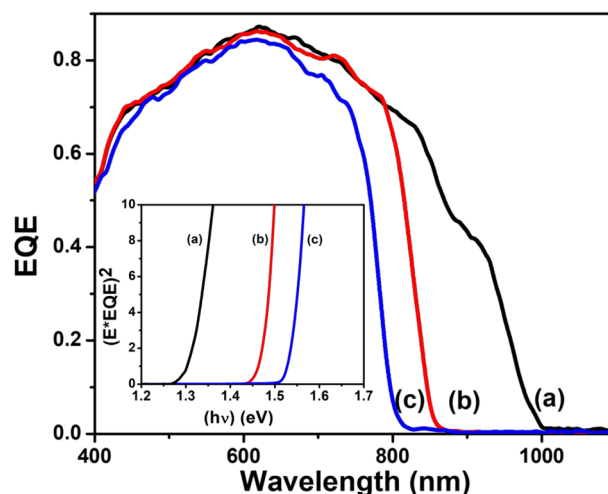

Fig. 11. External Quantum Efficiency measurement curves for (a) CIS, (b) CIGS and (c) CGS NPs solar cells. Inset shows the graph of $(E \times EQE)^2$ versus the photon energy.

Table 4

A summary of the solar cell parameters obtained for CIS, CIGS and CGS NPs devices under illuminated conditions.

Cell structure	V_{OC} (mV)	J_{SC} (mA/cm^2)	FF (%)	η %
Glass/FTO/CdS/CIS NPs/Au	549	33.00	43	7.80
Glass/FTO/CdS/CIGS NPs/Au	600	30.50	51	9.33
Glass/FTO/CdS/CGS NPs/Au	632	27.50	52	9.04

4. Conclusion

A controlled stoichiometric $CuIn_{1-x}Ga_xSe_2$ NPs are synthesized by using a simple low-cost, environment friendly chemical ion reduction method. The polyethylene glycol played a role of solvent as well as surfactant to control the growth of NPs. The insertion of Ga atoms into the crystal structure is examined by various analytical techniques. The $CuIn_{1-x}Ga_xSe_2$ samples exhibited tetragonal crystal structure with clear variation in 'd' values of respective Bragg reflections. The XRD results are further confirmed by HRTEM analysis. The 'd' values 3.45, 3.37 and 3.28 Å revealed by HRTEM are correspond (1 1 2) plane of

CIS, CIGS and CGS, respectively. The sharp spotted rings revealed from SAED pattern demonstrates the polycrystalline growth of $CuIn_{1-x}Ga_xSe_2$ NPs. The optical absorption results support the addition of Ga in the crystal structure with systematic blue shift in the absorption wavelength. Non-uniform $CuIn_xGa_{1-x}Se_2$ NPs of size ranging from 20 to 100 nm are observed from TEM analyses. However, upon annealing the final devices at 450 °C for 20 min. the NP layers become the polycrystalline alloy of materials with uniform cluster size between 100 and 200 nm. The superstrate solar cell devices developed with CIS, CIGS and CGS NPs measured PCE 7.80, 9.33 and 9.04%, respectively with input power intensity 100 mW/cm^2. The procedure reported for the synthesis of NPs using PEG is recommended to be highly suitable for fabrication of large area flexible thin film solar cell devices.

Declaration of Competing Interest

The authors declare that they have no known competing financial interests or personal relationships that could have appeared to influence the work reported in this paper.

Table 5

A comparative study of device parameters for $CuIn_{1-x}Ga_xSe_2$ NPs based solar cells fabricated.

Nanoparticles	Method of synthesis	Solar cell configuration	J_{sc}(mA/cm^2)	V_{OC} (V)	FF (%)	η (%)	Ref.
CIGSe	Colloidal	Mo/CIGS/CdS/ZnO/Ni-Al/MgF$_2$	27.1	0.518	32.6	4.6	Schulz et al. (1998)
CIS, CIGS and CGS	Colloidal	–	–	–	–	–	Gurin (1998)
CIGS	hot injection	Mo/CIGS/CdS/ZnO/ZnO:Al/Ni/Al/Ni	23.9	0.501	54	6.5	Barbé et al. (2016)
Cu(In,Ga)$_{0.5}$Se$_2$	Mechano-chemical Process (Ball milling)	–	–	–	–	–	Rohini et al. (2015)
CIS	hot injection	Mo/CIGS/CdS/i-ZnO/ITO	25.8	0.280	39	2.8	Guo et al. (2008)
CIGSSe	hot injection	SLG/Mo/CIGSSe/CdS/i-nO/ITO/Ni-Al	28.8	0.630	65.7	12.0	Guo et al. (2013)
copper indium gallium disulfoselenide (CIGSSe)	hot injection	Mo/CIGSSe/CdS/ZnO/ITO/Ni–Al grids/MgF2	32.1	0.630	73.4	15.0	McLeod et al. (2015)
CIGS	solvothermal	–	–	–	–	–	Kodigala (2010)
CIG(S,Se)	hot injection	Glass/Mo/CIGSSe/CdS/ZnO/ITO/Ag	27.36	0.420	36	4.2	Mousavi et al. (2016)
Z-doped CIS	hot injection	C/CIS/In2S3/TiO2/FTO/glass	23.70	0.594	50	7.53	Tuan et al. (2017)
CIGS	sonochemical route	Mo/CIGS/CdS/ZnO/ZnO:Al	2.35	0.242	37	0.2	CheshmeKhavar et al. (2017)
$CuIn_{1-x}Ga_xSe_2$ (x = 0, 0.5 and 1)	Chemical reduction method	Glass/FTO/CdS/CuIn$_{1-x}$Ga$_x$Se$_2$/Au	CIS = 33.0 CIGS = 30.50 CGS = 27.50	0.549 0.600 0.632	43 51 52	7.80 9.33 9.04	Present work

Acknowledgment

References

Ahn, S., Kim, K.H., Yun, J.H., Yoon, K.H., 2009. J. Appl. Phys. 105, 113533.
Alberts, V., Herberholz, R., Walter, T., Schock, H.W., 1997. J. Phys. D Appl. Phys. 30, 2156.
Badgujar, A.C., Dusane, R.O., Dhage, S.R., 2018. Vacuum 153, 191–194.
Barbé, J., Eid, J., Ahlswede, Erik, Spiering, Stefanie, Powalla, Michael, Agrawal, Rakesh, Del Gobbo, Silvano, 2016. J. Nanopart Res 18, 379.
Basol, B.M., Kapur, V.K., Leidholm, C., Halani, A., Minnick, A., 1996. In: AIP Conf. Proc., vol. 353, pp. 26.
Cassette, E., Pons, T., Bouet, C., Helle, M., Bezdetnaya, L., Marchal, F., Dubertret, B., 2010. Chem. Mater. 22, 6117–6124.
Cha, J.H., Noh, S.J., Jung, D.Y., 2015. Chem. Sus. Chem. 8, 2407–2413.
Chang, C.C., Chen, J.K., Chen, C.P., Yang, C.H., Chang, J.Y., 2013. ACS Appl. Mater. Interfaces 5, 11296–11306.
Chaure, N.B., Bordas, S., Samantilleke, A.P., Chaure, S.N., Haigh, J., Dharmadasa, I.M., 2003. Thin Solid Films 437, 10.
Chaure, N.B., Chaure, S., Pandey, R.K., 2004. Sol. Energ. Mater. Sol. Cell 81, 39.
Chen, W.S., Stewart, J.M., Devaney, W.E., Mickelsen, R.A., Stanbery B.J., 1993. In: 23rd IEEE Photovoltaic Specialists Conference, pp. 422.
CheshmeKhavar, A.H., Mahjoub, A.R., Taghavinia, N., 2017. Sol. Energy 157, 581–586.
Denton, A.R., Ashroft, N.W., 1991. Vegards Law. Phys. Rew. A 43, 3161–3164.
Egerton, Ray F., 2005. Physical Principles of Electron Microscopy, Springer, pp. 109–111.
Green, M.A., Dunlop, E.D., Hohl-Ebinger, J., Yoshita, M., Kopidakis, N., Ho-Baillie, A.W.Y., 2020. Prog. Photovolt. Res. Appl. 28, 3–15.
Guo, Q., Kim, S.J., Kar, M., Shafarman, W.N., Birkmire, R.W., Stach, E.A., Agarwal, R., Hillhouse, H.W., 2008. Nano Lett. 8, 2982–2987.
Guo, Q., Ford, G.M., Agrawal, R., Hillhouse, H.W., 2013. Prog. Photovolt. Res. Appl. 21, 64–71.
Gurin, V.S., 1998. Colloids Surf. A 142, 35–40.
Ishizuka, S., Sakurai, K. Yamada, A. , Matsubara, K., Fons, P., Iwata, K., Nakamura, S., 2004. In: 19th European Photovoltaic Solar Energy Conference, Paris, pp. 1729.
Kaelin, M., Rudmann, D., Tiwari, A.N., 2004. Sol. Energy 77, 749–756.
Kaelin, M., Rudmann, D., Kurdesau, F., Zogg, H., Meyer, T., Tiwari, A.N., 2005. Thin Solid Films 480–481, 486–490.
Kodigala S.R., 2010. Cu(In1-xGax)Se2 Based Thin Film Solar Cells, vol. 35, Elsevier Publishing.
Lebègue, E., Baranton, S., Coutanceau, C., 2011. J. Power Sources 196, 920–927.
Lee, W.D., Lim, D.H., Chun, H.J., Lee, H.I., 2012. Int. J. Hydrogen Energ. 37, 12629–12638.
Liu, C.P., Chuang, C.L., 2012. Powder Technol. 229, 78–83.
Liu, Y., Kong, D., Li, J., Zhao, C., Chen, C., Brugger, J., 2012. Energy Procedia 16, 217–222.
Londhe, P.U., Rohom, A.B., Chaure, N.B., 2015. RSC Adv. 5, 89635.
McDaniel, H., Fuke, N., Pietryga, J.M., Klimov, V.I., 2013. J. Phys. Chem. Lett. 4, 355–361.
McLeod, S.M., Hages, C.J., Carter, N.J., Agrawal, R., 2015. Prog. Photovolt: Res. Appl. 23, 1550–1556.
Mitzi, D.B., Yuan, M., Liu, W., Kellock, A.J., Chaey, S.J., Gignac, L., Schrott, A.G., 2009. Thin Solid Films 517, 2158–2162.
Mousavi, S.H., Müller, T.S., Karos, R., de Oliveira, P.W., 2016. J. Alloys Compd. 659, 178–183.
Noufi, R., Powell, R., Herrington, C., Coutts, T., 1986. Solar Cells 17, 303.
Panthani, M.G., Akhavan, V., Goodfellow, B., Schmidtke, J.P., Dunn, L., Dodabaapur, A., Barbara, P.F., Korgel, B.A., 2008. J. Am. Chem. Soc. 130, 16770–16777.
Peng, W., Du, J., Pan, Z., Nakazawa, N., Sun, J., Du, Z., Shen, G., Yu, J., Hu, J., Shen, Q., Zhong, X., Appl, A.C.S., 2017. Mater. Interfaces 9, 5328–5336.
Rohini, M., Reyes, P., Velumani, S., Latha, M., Goldieoza, I., Becerril-Juarez, R., 2015. Asomoza, Mater. Sci. Semi. Process. 37, 151–158.
Santaniello, E., Ferraboschi, P., Fiecchi, A., Grisenti, P., Manzocchi, A., 1987. J. Org. Chem. 52, 671–674.
Sargent, E.H., oleilat, G., Tang, J., Johnston, K.W., Pattantyus-Abraham, A.G., Konstantatos, G., Jacob DukenfieldKlem, E., Myrskog, S., MacNeil, D.D., Clifford, J. P., Levina, L., US20100044676A1,2010.
Schockley, W., Queisser, H.J., 1961. J. Appl. Phys. 32, 510–519.
Schulz, D.L., Curtis, C.J., Flitton, R.A., Wiesner, H., Keane, J., Matson, R.J., Jones, K.M., Parilla, Philip A., Noufi, R., Ginley, D.S., 1998. J. Electron. Mater. 27 (5), 433–437.
Septina, W., Gunawan, Ikeda, S., Harada, T., Higashi, M., Abe, R., Matsumura, M., 2015. J. Phys. Chem. C 119 (16), 8576–8583.
Tang, J., Hindos, S., Kelley, S.O., Sargent, E.H., 2008. Chem. Mater. 20, 6906–6910.
Thomas, S.R., Chen, C.W., Date, M., Wang, Y.C., Tsai, H.W., Wang, Z.M., Chueh, Y.L., 2016. RSC Adv. 6, 60643.
Tsuji, M., Hashimoto, M., Nishizawa, Y., Tsuji, T., 2004. Mater. Lett. 58, 2326–2330.
Tuan, A., Phan, V.N., Huy, T.D., Dung, D.V.A., Quang, N.X., Cuong, N.D., 2017. J. Electron. Mater. 46, 6.
Unold, T., Enzenhofer, T., Kaufmann, C.A., Klenk, R., Neisser, A., Sakurai, K., Schock, H. W., 2006. In: 4th World Conference on Photovoltaic Energry Conversion, pp. 356.
Wang, Y., Xia, Y., 2004. NanoLett 4, 2047–2050.
Wu, J., Wang, L.T., Gau, C., 2012. Sol. Energ. Mater. Sol. Cell 98, 404–408.
Wu, J., Lan, Z., Lin, J., Huang, M., Huang, Y., Fan, L., Luo, G., Lin, Y., Xie, Y., Wei, Y., 2017. Chem. Soc. Rev. 46, 5975.
Xiao, J., Xie, Y., Tang, R., Qian, Y., 2001. J. Solid State Chem. 161 (2), 179–183.